Available online at www.sciencedirect.com
ScienceDirect
Journal of Magnetic Resonance 182 (2006) 12–21
JMR Journal of Magnetic Resonance
www.elsevier.com/locate/jmr

# Spatially encoded pulse sequences for the acquisition of high resolution NMR spectra in inhomogeneous fields

Boaz Shapira, Lucio Frydman *

*Department of Chemical Physics, Weizmann Institute of Science, 76100 Rehovot, Israel*

Received 31 January 2006; revised 17 April 2006
Available online 27 June 2006

**Abstract**

We have recently proposed a protocol for retrieving nuclear magnetic resonance (NMR) spectra based on a spatially-dependent encoding of the MR interactions. It has also been shown that the spatial selectivity with which spins are manipulated during such encoding opens up new avenues towards the removal of magnetic field inhomogeneities; not by demanding extreme $B_o$ field uniformities, but rather by compensating for the dephasing effects introduced by the field distribution at a radiofrequency excitation and/or refocusing level. The present study discusses in further detail a number of strategies deriving from this principle, geared at acquiring both uni- as well as multi-dimensional spectroscopic data at high resolution conditions. Different variants are presented, tailored according to the relative sensitivity and chemical nature of the spin system being explored. In particular a simple multi-scan experiment is discussed capable of affording substantial improvements in the spectral resolution, at nearly no sensitivity or scaling penalties. This new compensation scheme is therefore well-suited for the collection of high-resolution data in low-field systems possessing limited signal-to-noise ratios, where magnetic field heterogeneities might present a serious obstacle. Potential areas of applications of these techniques include high-field in vivo NMR studies in regions near tissue/air interfaces, clinical low field MR spectroscopy on relatively large off-center volumes difficult to shim, and ex situ NMR. The principles of the different compensation methods are reviewed and experimentally demonstrated for one-dimensional inhomogeneities; further improvements and extensions are briefly discussed.


*Keywords:* High resolution NMR; Spatial encoding; Field inhomogeneity; Susceptibility compensation

## 1. Introduction

Nuclear magnetic resonance spectroscopy can deliver unique chemical insight in a non-invasive fashion [1]. To do so, however, it demands an extremely high homogeneity from the external magnetic field $B_o$ where the experiment takes place. Field inhomogeneities $\Delta B_o(r) = \gamma\Omega_{\text{inh}}(r)$ need to be reduced until made small vis-à-vis the smallest internal shifts or couplings to be measured, when considered over the full sample volume. This translates in demanding that field perfections be better than 1 part in $10^8$ over sample volumes on the order of 1 $\text{cm}^3$; a significant challenge requiring serious investments in both the size of the main magnet and the number of auxiliary shimming coils to be used [2]. Moreover instances arise where even the most extensive efforts cannot deliver the required field homogeneity; for example when dealing with samples subject to substantial internal susceptibility distortions, or when dealing with sudden changes in the medium being examined. All of these are common scenarios in a variety of in vivo NMR spectroscopy experiments [3], where the achievement of high resolution is further aggravated by the relatively low length-to-width ratio of the typical animal or clinical magnet, and by the advent of higher magnetic field strengths requiring an increasing number of higher-order shims to achieve the needed field corrections. An ultimate example of these complications is found in ex situ NMR experiments, whose goal is to obtain high resolution spectroscopic information from objects operating on the basis of single-sided magnets [4].

* Corresponding author. Fax: +972 8 9344123.
*E-mail address:* lucio.frydman@weizmann.ac.il (L. Frydman).

1090-7807/$ - see front matter © 2006 Elsevier Inc. All rights reserved.
doi:10.1016/j.jmr.2006.04.012

In an effort to overcome these complications, a number of alternatives have been proposed for collecting high resolution chemical information in the presence of field distortions. One of the first strategies to be demonstrated involved the use of two-dimensional (2D) NMR experiments, where high resolution was achieved by correlating the effects of arbitrary field inhomogeneities at a particular chemical site with identical effects affecting neighboring sites in the spin system [5,6]. While the reliance of these experiments on relatively weak multi-spin correlations did not endow them with the highest of sensitivities, they showed an advantage over competing proposals in that they dealt equally well with 1D, 2D or 3D $\Omega_{\text{in}}(r)$ distributions. These 2D correlations have therefore served as basis for a variety of high-resolution NMR experiments in inhomogeneous fields [7,8]. Another compensation approach to remove field inhomogeneities proposed the use of custom-built radiofrequency (RF) coils, whose $B_1$ distortions matched spatially those of the $B_o$ field [9,10]. Recently a different route for exploiting RF fields to compensate for $\Delta B_o$ inhomogeneities possessing a priori arbitrary spatial dependencies has been described; this involved the combined application of a field gradient spreading out the spins resonance frequencies according to their spatial positions, in conjunction with a suitable train of excitation or refocusing RF pulses whose phases compensate for the cumulative effects of the inhomogeneities [11,12]. Worth mentioning in connection to this approach yet in a fast-imaging context is also the use of tailored-RF excitation pulses applied in combination with a slice-selection gradient, in order to compensate for susceptibility distortions arising in echo-planar-imaging acquisitions at the instant of the main gradient-echo formation [13,14].

The purpose of the present work is to further discuss the potential of these gradient-assisted spatially encoded manipulations, towards the acquisition of high resolution NMR spectra in inhomogeneous or unstable fields. To do so we focus mostly on static one-dimensional inhomogeneities, and proceed to extend the basic spatial encoding framework laid out in our previous Communication [11] to describe a variety of compensating sequences. These include a spatially-continuous indirect-domain single-scan compensation approach, a new kind of "shim pulse" somewhat different in nature from those recently discussed by Pines et al. [12], and a novel class of multi-scan 2D compensation experiments. We illustrate applications of these techniques with 1D and 2D NMR acquisitions, stressing their usefulness and potential as well as their respective limitations. In particular it is shown that the last of the approaches mentioned can considerably alleviate the complications associated to hitherto available sequences, both in terms of the achievable resolution as well as of spectral sensitivity. Possible extensions of all the assessed methods to deal with inhomogeneities in multiple spatial/temporal dimensions, are also briefly discussed.

## 2. Single-scan strategies for the acquisition of high resolution NMR data in inhomogeneous fields

The principle by which spatially-encoded RF-based corrections can compensate for field inhomogeneities, is relatively straightforward. Consider a field inhomogeneity profile $\Delta B_o(t) = \gamma\Omega_{\text{inh}}(r,t)$ that has been a priori characterized, acting in simultaneity with a set of internal frequencies $\Omega_1$—stemming for instance from chemical shifts or $J$-couplings—whose spectral distribution $I(\Omega_1)$ we are attempting to measure. A conventional excitation will lead in the transverse rotating-frame plane to a uniformed-phase spin density profile $\rho$, which in the absence of relaxation will result in a time-domain signal

$$S(t) \propto \sum_{\Omega_1} I(\Omega_1) \mathrm{e}^{\mathrm{i}\Omega_1 t} \int_{\text{all } r} \rho \cdot \mathrm{e}^{i\Omega_{\text{inh}}(r,t)t} \mathrm{d}^3 r. \tag{1}$$

In general this signal will decay within a timescale that is inverse to $\Omega_{\text{inh}}$'s span over the detected volume of interest, precluding a resolution of $\Omega_1$ interactions situated closer than this spread. By contrast if one departs from a uniform spin excitation and replaces it with a phase-encoded $\rho(\boldsymbol{r},t) = \rho_o \exp[\mathrm{i}\phi(\boldsymbol{r},t)]$ state where $\phi(\boldsymbol{r},t) = -\Omega_{\text{inh}}(\boldsymbol{r},t)t$, it is clear that the resulting time-domain signal will be free from the effects of the inhomogeneity and therefore solely reflective of the internal interactions. From an analysis of $S(t)$ a high-resolution, inhomogeneity-free $I(\Omega_1)$ spectrum would follow. This simple argument highlights the two main challenges to overcome towards the successful exploitation of this approach: (i) an optimal strategy for imparting for a given time $t$ the spatially-selective $z$-rotation represented by $\phi(\boldsymbol{r},t) = -\Omega_{\text{inh}}(\boldsymbol{r},t)t$ needs to be designed, and (ii) a way of extending the single-instant correction imparted by this $\phi(\boldsymbol{r},t)$ towards the acquisition of a *full* $S(t)$ set multiplexing all spectral information, needs to be found. The latter appears to be the main of the two challenges, particularly if one wishes to implement it on a single-scan acquisition basis. Yet two examples have recently exemplified the use of spatially-selective manipulations of the kind just described, to the acquisition of high resolution data within a single scan [11,12]. Section 2 is devoted to a theoretical description of these methods, and to the experimental demonstration of their potential and limitations.

### 2.1. Single-scan strategies based on an indirect-domain spatial encoding of the corrections

One of the solutions proposed for achieving the high resolution goals just mentioned exploited the principles involved in single-scan nD NMR [15,16]. By already relying on a spatially-resolved encoding of the spin interactions, this methodology provides a natural starting point for a $\phi(\boldsymbol{r})$-based inhomogeneity compensation. Unlike what happens in conventional time-domain experiments, single-scan nD NMR delivers its high-resolution

spectroscopic information within an acquisition time $T_a$ that can in principle be made arbitrarily short. This is the consequence of a read-out process where peak positions become determined by the action of an acquisition gradient $G_a$ defining spectral widths according to a wavenumber $k = \gamma \int_0^t G_a(t')\mathrm{d}t'$, rather than as a result of the numerical Fourier transform of an $S(t)$ time-domain signal. Thus in the usual case of a square-wave gradient acquisition, the spatially-encoded spectral width reaches a maximum span of $\gamma G_a T_a$ and allows one to arbitrarily shorten the acquisition time by a concomitant increase in the gradient's strength. This in turn helps solve the single-instant multiplexing issue mentioned above. We summarize next how spatial encoding enables the acquisition of high resolution spectra assuming, for simplicity, a static inhomogeneity that is unidimensional in nature.

A number of strategies have been proposed for achieving the spatial encoding underlying single-scan nD NMR [15–20]. One of these relies on a series of $N_1$ discrete excitation pulses, that trigger the evolution of spins placed at different positions $\{r_i\}_{i=1,N_1}$ over a series of incremented times $t_1(r_i) = C(r_i - r_{N_1})$ (Fig. 1A). In order to implement such spatially-selective excitation a suitably refocused encoding gradient $G_e$ is activated, and the offset $\{O_i\}_{i=1,N_1}$ of the excitation pulses is evenly spread between the $\pm\gamma G_e L/2$ frequency bounds dictated by the sample length $L$ [16]. In the presence of the inhomogeneities, individual positions $r_i$ are then addressed by this train of RF excitation pulses according to

$$O[t_1(r_i)] = \gamma G_e r_i + \Omega_{\mathrm{inh}}(r_i). \tag{2}$$

This is correct within an undetermined error $\delta r \approx \Omega_1/\gamma G_e$ given by the a priori unknown off-resonance values—an error which for simplicity we shall assume small. The overall position-dependent phase $\phi_e(r_i)$ accumulated by the spins following such discrete spatial encoding process will then reflect a free evolution, depending on the internal shifts $\Omega_1$ as well as on the inhomogeneity effects one is trying to remove:

$$\phi_e(z_i) = \phi_{\mathrm{RF}}(r_i) + t_1(r_i)[\Omega_1 + \Omega_{\mathrm{inh}}(r_i)]; \quad i = 1, \ldots, N_1. \tag{3}$$

Here, $\phi_{\mathrm{RF}}(r_i)$ denotes the relative phase of the RF pulse used to excite the $i$-th discrete spin-packet, and is a key parameter that we can freely manipulate to remove the apparent effects of the inhomogeneity. Indeed since both $\Omega_{\mathrm{inh}}(r)$ and $t_1(r_i)$ are known functions, setting the phases of the RF pulses equal to $\phi_{\mathrm{RF}}(r_i) = -t_1(r_i)\ \Omega_{\mathrm{inh}}(r_i)$ (within an arbitrary constant value) will ensure that the overall encoding stemming from Eq. (3) ends up free from the effects of the field inhomogeneity, yet reflective of the $\Omega_1$ evolution to be measured [11].

As mentioned, a number of alternatives to this discrete option have been proposed for implementing the spatial encoding underlying single-scan 2D NMR. These include the application of pairs of chirped π/2 pulses [17], pairs of adiabatic π pulse sweeps [18] and π/2–π pulse combinations [19,20]; all of these acting while under the action of suitable field gradients and capable of yielding the linear $C\Omega_1(r - r_o)$ encoding required for the subsequent $G_a$-driven readout of the interactions. Like their discrete counterpart all these continuous alternatives possess an inhomogeneity compensation potential; given the advantages of these frequency-swept options, we address next their mode of compensation. For simplicity we shall focus on the π/2–π/2 combination (Fig. 1B), an experiment where continuously swept RF pulses are applied twice: first over an initial time $t_p^+$ to effect a progressive excitation of the spins, and then over a final time $t_p^-$ to implement a regressive storage of the transverse evolution. As a result of these pulses an amplitude modulation is created, encoding the $t_1$ effects of the shifts and couplings as a spatial pattern of stored magnetizations. In the usual, homogeneous field scenario, the offset of these two chirped pulses is swept over the relevant $|\gamma G_e L|$ frequency intervals at a constant rate $R \approx 2\gamma G_e L/t_1^{\max}$ during equal periods $t_p^+ = t_p^- = t_1^{\max}/2$, while the sign of $G_e$ is alternated between the excitation and storage. It can then be shown that by setting the RF intensity $\gamma B_1 \approx 0.25\sqrt{R}$ identical π/2 nutations are achieved; the resulting amplitude-modulated signal possesses the kind of pattern required by the spatial encoding procedure [17]. In order to derive the conditions under which such pair of pulses will deliver the same $\phi_e(r) = C\Omega_1(r - r_o)$ spin evolution even in the presence of

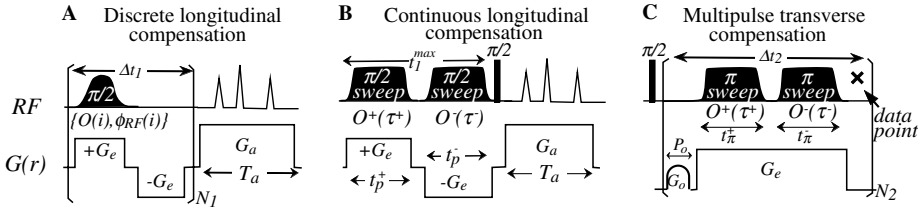


Fig. 1. Strategies capable of yielding high resolution spectra with compensated field inhomogeneities within a single scan, by means of the combined application of shaped RF pulses and refocused field gradients. (A) Discrete spatially-encoded strategy illustrated in Ref. [11], yielding a compensated $t_1$ evolution by means of RF phase manipulations. (B) Scheme relying on shaping the offset of two continuously-chirped RF pulses, and imposing an $\Omega_{\mathrm{inh}}$-compensated longitudinal pattern at the conclusion of the indirect domain evolution. (C) Direct-domain compensation scheme involving the application of two consecutive adiabatic inversions plus an extra linear gradient, shaped so as to refocus inhomogeneities within each dwell time $\Delta t_2$. Unlike cases (A) and (B), where data digitized over a time $T_a$ will directly furnish the desired spectrum (illustrated by the peaks in the cartoons), (C) requires a Fourier transform of the data for the sake of delivering the spectral information.

field inhomogeneities, we shall consider as in the discrete case a 1D problem where once again $\|\gamma G_e L\| \gg \|\Omega_1\|$. The first of these pulses will then address spins progressively at times $\tau^+(r)$ when its RF offset $O^+$ matches the spin's resonance frequency $\omega^+(r) = \gamma G_e^+ r + \Omega_{\text{inh}}(r)$; the second one will act at a time $\tau^-(r)$ when its offset $O^-$ matches $\omega^-(r) = \gamma G_e^- r + \Omega_{\text{inh}}(r)$. Following an extension of Eq. (3), the overall phase that gets evolved by the spins' magnetizations as a function of their position will be given by

$$\phi_e(r) = [t_p^+ - \tau^+(r)]\omega^+(r) + \tau^-(r)\omega^-(r) + \phi_{\text{RF}}[\tau^+(r)] - \phi_{\text{RF}}[\tau^-(r)]. \tag{4}$$

The first two terms in this expression denote the free evolution undergone by spins as a result of the gradient and of the inhomogeneity; as these are both artifacts of the experiment, our aim will be to remove them. To do so we shall be aided by the two $\phi_{\text{RF}}$ terms in Eq. (4)'s right-hand side, which are added and subtracted from the spins' evolution by the excitation and storage pulses respectively. These latter contributions can be summarized as

$$\phi_{\text{RF}}[\tau^{\pm}(r)] = \int_0^{\tau^{\pm}(r)} O^{\pm}(\tau')\mathrm{d}\tau', \tag{5}$$

where, as in Eq. (2), $O^{\pm}[\tau(r)] = \gamma G_e^{\pm} r + \Omega_{\text{inh}}(r)$. Notice that in comparison with the discrete refocusing case Eq. (5) places an additional constraint, given by the fact that in a continuous sweep scenario the offsets and phases of the RF encoding pulses can no longer be independently manipulated. One possible way to bypass such constraint could rely on the gradients, making the $G_e^{\pm}$ time-dependent in such fashion so as to compensate for the $\Omega_{\text{inh}}(r)$. Instead we shall follow the approach described in Ref. [21] and keep the gradients time-independent, yet depart from the constant sweep rate condition and exploit the variability that modulating the $\tau^{\pm}(r)$'s offers to tailor the phase imparted on the spins as a function of position.

The inhomogeneity refocusing condition can be summarized by requesting that Eq. (4) be deprived of its spatial dependence; i.e., by claiming

$$\frac{\mathrm{d}\phi_e(r)}{\mathrm{d}r} = 0. \tag{6}$$

Simultaneously, the RF sweeps leading to this condition need to allow for a linear spatial encoding of the internal interactions; in other words the overall free evolution time $t_1$ must, as in the homogeneous $B_o$ situation, fulfill

$$t_1(r) = [t_p^+ - \tau^+(r)] + \tau^-(r) = C(r_o - r) \tag{7}$$

with $C = t_1^{\max}/L$ and $r_o = -L/2$. Eqs. (4)–(7) suffice to derive the times $\tau^{\pm}(r)$ at which the continuously-swept RF offsets have to excite/store spin coherences positioned at a given coordinate $r$, and at the same time remove the effects of the inhomogeneity. Assuming for simplicity that as in the homogeneous encoding cases one uses $G_e^+ = -G_e^- = G_e$, these conditions can be shown to lead to

$$\tau^+(r) = \frac{C}{2\gamma G_e}\left\{-L\left.\frac{\mathrm{d}\Omega_{\text{inh}}}{\mathrm{d}r}\right|_{r=r_o} + \left(\frac{L}{2} - r\right)\left[\gamma G_e - \frac{\mathrm{d}\Omega_{\text{inh}}(r)}{\mathrm{d}r}\right]\right\} \tag{8a}$$

and

$$\tau^-(r) = \frac{C}{2\gamma G_e}\left(\frac{L}{2} + r\right)\left[\gamma G_e + \frac{\mathrm{d}\Omega_{\text{inh}}(r)}{\mathrm{d}r}\right]. \tag{8b}$$

From these expressions the frequency sweep profiles of the encoding pulses can be obtained by inverting $\tau^{\pm}(r)$ into $r(\tau^{\pm})$ (numerically if need be), and by then plugging the resulting function into the frequency-modulated excitation/storage profiles $O^{\pm}(\tau) = \pm\gamma G_e r(\tau^{\pm}) + \Omega_{\text{inh}}[r(\tau^{\pm})]$. As in the homogeneous case a suitable amplitude modulation of such frequency-shaped pulses also needs to be introduced, so that the adiabaticity parameters of the sweeps keep on maintaining the $\gamma B_1(\tau) \approx 0.25\sqrt{|\mathrm{d}O(\tau)/\mathrm{d}\tau|}$ condition required for imparting $\pi/2$ nutations [17]. Notice that as a result of the inhomogeneity the durations of the swept pulses cease to be identical, and become instead given by the

$$\frac{t_p^-}{t_p^+} = \frac{\gamma G_e + \left.\frac{\mathrm{d}\Omega_{\text{inh}}}{\mathrm{d}r}\right|_{r=r_o}}{\gamma G_e - \left.\frac{\mathrm{d}\Omega_{\text{inh}}}{\mathrm{d}r}\right|_{r=r_o}} \tag{9}$$

ratio. Further conditions that $\Omega_{\text{inh}}(r)$, $\gamma G_e$ need to fulfill in order to enable an inversion of Eq. (8) into an RF frequency profile, are discussed in Ref. [21].

### 2.2. Single-scan strategies based on spatially-dependent direct-domain rotations: shim pulses

The strategies just described amount to shaping the RF excitation/storage pulses, so as to impart spatially-dependent $z$-rotations that at the conclusion of an in indirect time $t_1$ shall be able to remove known inhomogeneity profiles. Spatially-dependent $z$-rotations can also be used in an alternative way to remove previously-known field inhomogeneities; namely, by applying them on spins *after* they have been excited into the transverse $x$–$y$ plane. This results in "shim pulses"; spatially-dependent rotations designed to refocus the effects of inhomogeneities acting within a particular dwell time $\Delta t_2$ while preserving, at least to some extent, the effects of chemical shifts. As discussed in Ref. [12] a pair of consecutive $\pi$ pulses spanning the shortest possible times $t_\pi^+$, $t_\pi^-$ and applied in-between the signal digitization, provide a particularly simple way to impart this kind of spatially-selective $z$-rotations (Fig. 1C). Indeed as each $\pi$ pulse reverses the effects of the chemical shifts (while leaving homonuclear couplings unaffected) a spectrum will result where chemical shifts appear scaled by a factor $\frac{t_\pi^+ + t_\pi^-}{t_\pi^+ + t_\pi^- + \Delta t_2}$, while the $J$-coupling strengths remain unchanged. From a practical perspective this approach differs and complements the one given in the previous paragraph, in the sense that instead of compensating inhomogeneities only once and over an indirectly-monitored delay $t_1^{\max}$, it operates a number $N_2$ of times equaling the number of digitized

points, imparting at every instance a correction corresponding to the evolution time $\Delta t_2$. Aside from the practical consequences that these differences in implementation have, the description underlying the transverse shim-pulse correction is similar to the one given earlier for the longitudinal spatial encoding scenario. We thus extend here the analysis just given based on the π/2–π/2 procedure, to the case of an inhomogeneity refocusing implemented by a pair of frequency-chirped π–π pulses acting while in the presence of pulsed gradients.

Following arguments given elsewhere concerning the use of adiabatic π sweeps to obtain spatially-encoded signals [18–21], we can describe the overall phase evolved during the course of each of transverse dwell time $\Delta t_2$ in Fig. 1C as

$$\phi_e(r) = \phi_\pi^-(r) - \phi_\pi^+(r) + \phi_{\mathrm{inh}}^-(r) + \phi_{\mathrm{inh}}^+(r). \tag{10}$$

Here, the functions

$$\phi_\pi^\pm(r) = -\tau^\pm(r)\omega^\pm(r) + 2\phi_{\mathrm{RF}}^\pm[\tau^\pm(r)] + \left[t_\pi^\pm - \tau^\pm(r)\right]\omega^\pm(r) \tag{11}$$

denote the phase evolutions that in the rotating frame of reference the two consecutive π inversions lasting times $t_\pi^\pm$ will impart, while the

$$\phi_{\mathrm{inh}}^\pm(r) = \left[\frac{\Delta t_2}{2} - t_\pi^\pm\right]\Omega_{\mathrm{inh}}(r) \tag{12}$$

terms describe the effects of the inhomogeneities to be compensated, acting before the first and after the last of the chirped π pulses. Notice that if the two pulses are identical Eq. (11) predicts that their net effect will be zero, meaning that they will have to differ from one another if the $\phi_{\mathrm{inh}}^\pm$ effects are to be compensated. Inhomogeneity effects can then be removed either by manipulating the gradients (included in the $\omega^\pm$'s), or by manipulating both the gradients as well as the phase patterns that are imparted by the RF pulses. Pines et al. have presented within a numerical framework applications of the first of these corrective choices; instead, and as was the case for the treatments presented above, we chose to focus on the opportunities opened up by tailoring the offset-driven $\phi_{\mathrm{RF}}^\pm$ terms appearing in Eq. (11). Since once the burden of the $\Omega_{\mathrm{inh}}$ correction is switched onto the RF the gradient shapes to be used remain to be defined, we assumed for the sake of experimental simplicity that these were equal over the course of the π pulses. In other words, we made $\omega^+(r) = \omega^-(r) = \gamma G_e r + \Omega_{\mathrm{inh}}(r)$ for the two consecutive π sweeps. It can then be shown that a small additional gradient becomes necessary to enable the presence of a period of free evolution (i.e., to break the trivial $t_\pi^+ = t_\pi^- = \Delta t_2/2$ high resolution condition); this was introduced in the form of a small $k_o = G_o P_o$ gradient pulse adding an overall additional phase $k_o r$ (Fig. 1C). When applied to the scenario posed by Eqs. (10)–(12) the inhomogeneity-compensated evolution conditions then demands

$$\begin{aligned}\frac{\mathrm{d}\phi_e(r)}{\mathrm{d}r} &= \left[\Delta t_2 - t_\pi^+ - t_\pi^-\right]\frac{\mathrm{d}\Omega_{\mathrm{inh}}}{\mathrm{d}r} \\ &\quad + 2\left\{\left[\tau^+(r) - \frac{t_\pi^+}{2}\right] - \left[\tau^-(r) - \frac{t_\pi^-}{2}\right]\right\}\left[\gamma G_e + \frac{\mathrm{d}\Omega_{\mathrm{inh}}}{\mathrm{d}r}\right] \\ &= k_o. \end{aligned} \tag{13}$$

A redundancy arises here in control variables, given by the fact that either the $\tau^+(r)$ or $\tau^-(r)$ functions (i.e., either one of the RF sweeps originating $\phi^+$ and $\phi^-$) could in principle be modulated for the sake of compensating out the effects of $\Omega_{\mathrm{inh}}(r)$. To further determine this problem we chose a symmetric-like solution, where the compensating tasks are equally split between the two π sweeps. This in turn leads to the functions

$$\tau^\pm(r) = \frac{t_\pi^\pm}{L}(r + L/2) \pm \delta\tau(r). \tag{14}$$

The boundary conditions $\tau^+(-L/2) = \tau^-(-L/2) = 0$; $\tau^+(+L/2) = t_\pi^+$; $\tau^-(+L/2) = t_\pi^-$ can then be used to define the length of the pulses and gradients to be used for a given inhomogeneity profile and $\Delta t_2$ value; with these parameters at hand the correcting functions can be derived as

$$\delta\tau(r) = \frac{k_o + \frac{\mathrm{d}\Omega_{\mathrm{inh}}(r)}{\mathrm{d}r}\left[t_\pi^+ + t_\pi^- - \Delta t_2\right]}{4\left[\gamma G_e + \frac{\mathrm{d}\Omega_{\mathrm{inh}}(r)}{\mathrm{d}r}\right]} - \frac{\left(t_\pi^+ - t_\pi^-\right)z}{2L}. \tag{15}$$

As in the case of the longitudinal compensation these demands can be inverted to derive the $r(\tau^\pm)$ functions, from which the offset frequency shapes $\phi^\pm = O[r(\tau^\pm)]$ follow. Also in this instance, the amplitudes of the resulting RF sweeps need to be tailored to fulfill in all cases the adiabaticity demands of π inversions.

### 2.3. An experimental comparison of methods

In order to evaluate the refocusing performance of the inhomogeneity compensation approaches introduced in the preceding paragraphs, a series of simple tests were carried out on a Varian INova® 501 MHz spectrometer utilizing the $^1$H NMR spectrum of a *n*-butylchloride/$CDCl_3$ solution as target. Under normal high-resolution conditions the four individual chemical sites and the mutual $^1$H–$^1$H *J*-couplings within this compound are clearly visible (Fig. 2A). An uniaxial field inhomogeneity was mimicked by setting the various spectrometer *z* shim currents to arbitrary values, leading to a continuous $^1$H lineshape containing few discernible site-related features. Still, a conventional mapping of the sites' resonance frequencies vs position had no difficulties in revealing the $\Omega_{\mathrm{inh}}(\hat{z})$ inhomogeneity profiles for every site (Fig. 2B). Using such artificially broadened spectrum as starting point (Fig. 3A) the strategies sketched in Figs. 1B and C were assayed (results arising from the approach in Fig. 1A are not hereby presented as they have already been illustrated in Ref. [11]). Fig. 3B shows the kind of resolution improvement obtained with the longitudinal corrective scheme in Fig. 1B. The indirect-domain spatially-encoded

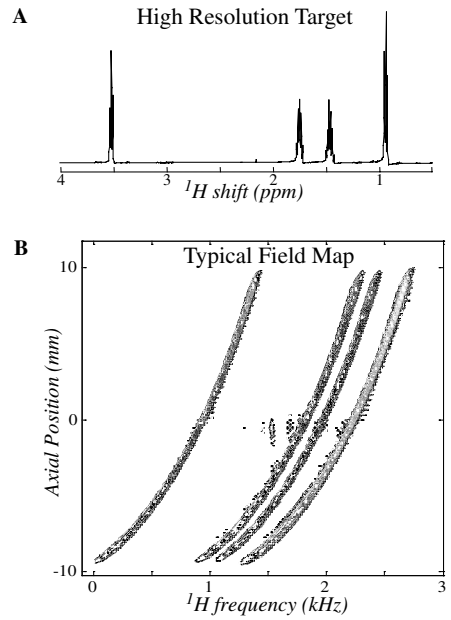


Fig. 2. (A) High-resolution $^1$H NMR spectrum of the *n*-butylchloride/$CDCl_3$ solution used as target for assaying the $\Omega_{inh}$ compensation procedures. (B) Example of the artificial broadening introduced by missdialing the $\{\hat{z}^i\}_{i=1-5}$ values in the spectrometer's shim coils, shown as plots of the frequency of each site vs its axial position within the sample.

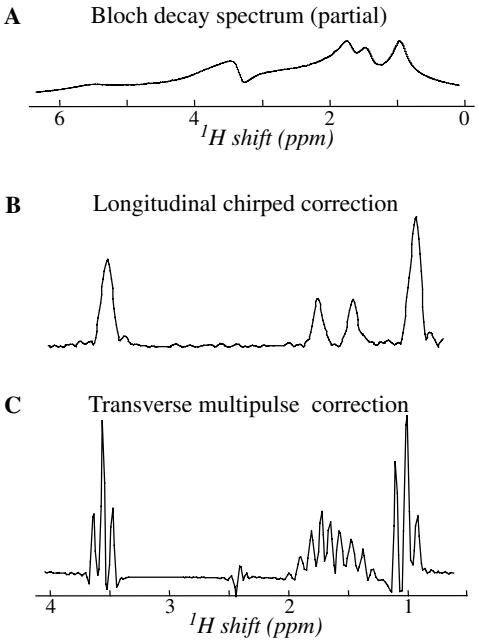


Fig. 3. Experimental demonstration of the performance of the single-scan schemes illustrated in Figs. 1B and C, to compensate for 1D $\Omega_{inh}(r)$ inhomogeneities. (A) Artificially broadened spectrum of the target sample obtained following a single-pulse $\pi/2$ excitation. (B) Results from the $\pi/2$–$\pi/2$ continuous spatial encoding along $t_1$. (C) Idem but for a train of $\pi$–$\pi$ corrections applied in-between each sampled point along $t_2$. See text for further details.

compensation employed a $t_1^{max} \approx 40$ ms, two $\pi/2$ chirped pulses applied while in the presence of a $|G_e| = 10$ G/cm encoding gradient along the $\hat{z}$ direction, and a data decoding period $T_a = 0.4$ ms under the action of a $G_a = 10$ G/cm acquisition gradient. Arguably, a stronger encoding gradient could have lead to smaller shift-induced errors in the inhomogeneity correction, which for the present case were given by $\|\Delta\Omega_{cs}/\gamma G_e\| \approx 0.1$ mm. On the other hand stronger gradients would also have exacerbated the potential effects of diffusion over the course of $t_1$. The effective half line width observed for the peaks in this corrective experiment was ca. 30 Hz; sufficient to unambiguously resolve the inequivalent chemical sites, yet not their internuclear spin–spin couplings.

Fig. 3C illustrates a second set of results, this time obtained with the transverse shim-pulse corrections of Fig. 1C. Constant 10 G/cm gradients were used in this compensation, acting in unison with ≈1.5 ms long frequency-tailored $\pi$ pulses. These dual RF sweeps were chirped over a 100 kHz range; ≈10% outside the observation region $L$ (≈1.90 cm) in order to avoid potential edge effects. Following these corrections a 0.5 ms window free of RF and incorporating the required $k_o$ correction ($-0.327$ cm$^{-1}$) were introduced in order to enable a chemical shift encoding by the spins, followed by the acquisition of a high-resolution $t_2$ data point. A total of 64 such $\pi$ pulses/data acquisition modules were employed, leading to an overall acquisition time of 224 ms. This kind of direct-domain spatial correction procedure clearly allowed us to resolve the homonuclear *J*-couplings, with effective line widths decreasing from ≈1500 Hz to about 4 Hz. On the other hand, the fact that out of the 224 ms acquisition time only ≈32 ms took place under conditions of free evolution, lead to a substantial scaling of the apparent chemical shifts effects—with the spectrum taking the appearance of data recorded at a 75 MHz Larmor frequency, rather than at 501 MHz. As pointed out earlier, this reflects the fact that the shift evolution freezes over the course of the $\pi$–$\pi$ compensations, whereas the *J*-coupling evolution proceeds nearly unhindered over the full length of $t_2$.

The two inhomogeneity refocusing solutions just described are in a way complementary: one operates by spatially encoding its compensations along an indirect $t_1$ evolution domain, while the other refocuses inhomogeneities in-between $\Delta t_2$ direct-domain dwell times. A natural approach to try out is consequently to combine both 1D refocusing strategies, so as to explore new opportunities towards the acquisition of *two-dimensional* NMR spectra in inhomogeneous fields. Indeed neither of the two corrective approaches just described makes any special demands on the evolutions that might have occurred in a complementary time-domain space, thereby allowing for their natural integration without substantial additions or modifications. Fig. 4 illustrates results obtained from such combination, using once again the conditions of Fig. 2 as an example. Notice that the resulting 2D spectra, which exhibit a remarkable high resolution along their two dimensions, are in all cases the result of single-scan acquisition experiments.

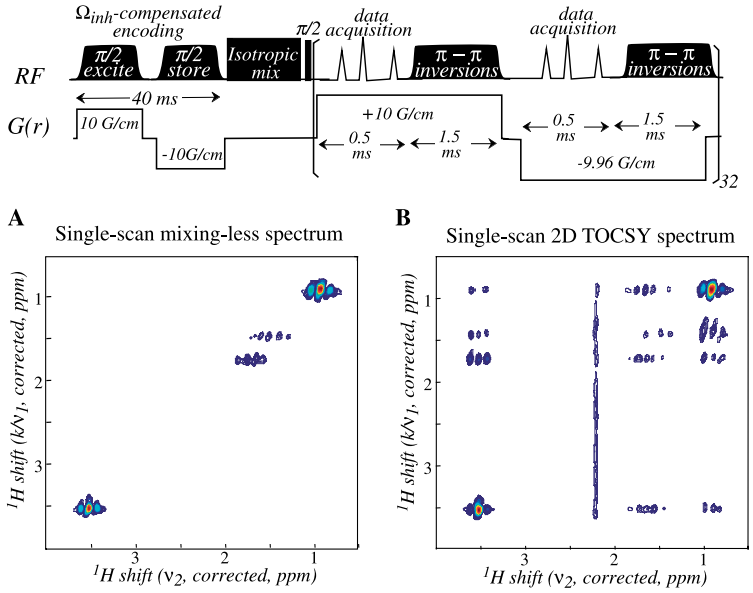


Fig. 4. Examples of data sets collected upon merging the strategies illustrated in Figs. 1B and C, into the unified single-scan 2D acquisition scheme shown on top. (A) Mixing-less trace displaying a purely diagonal correlation. (B) Idem upon introducing a 60 ms long DIPSI-based isotropic mixing period. Experimental parameters were identical as those mentioned in connection to Fig. 3; the different appearances along the indirect- and direct-domains are mostly a consequence of the different scalings characterizing the two $\Delta B_o$ compensation sequences.

## 3. Extensions to multiple-scan acquisition strategies

The spatially-selective encoding strategies described above can sharpen up spatially inhomogeneous NMR peaks by orders of magnitude. Yet as the experimental results also illustrate, these approaches face a number of limitations in delivering an optimum chemical shift information. The main limitation of the indirect-domain spatial encoding approach concerns—as is also the case for single-scan 2D NMR—the issue of sensitivity. Indeed although a variety of manipulations and optimizations could lead to a resolution that exceeds the one exemplified in Fig. 3B, such experiments would demand that the actual acquisition time of the data ($T_a$) be made much shorter that the decay time introduced by the inhomogeneity. And although this can always be achieved by employing a sufficiently large acquisition gradient $G_a$, a price has to be paid in terms of a larger filter bandwidth (proportional to $\gamma G_a L$) and of a stronger ensuing noise affecting the data. These sensitivity penalties have been discussed in further detail elsewhere [22]. As for the direct-domain compensation approach, it's main drawback appears to stem from the substantial scaling of the chemical shifts on which it incurs (Fig. 3C). Once again it seems likely that a number of optimizations could be here implemented to reduce the duration taken by the $z$-rotations—for instance by applying the two refocusing π pulses in near simultaneity rather than in the sequential fashion depicted in Fig. 1. Still it is not evident that the resulting improvements could enable the routine use of the compensation towards chemical shift-based identifications, particularly in the relatively low fields normally associated to MR spectroscopy in wide bore animal or clinical scanners.

And yet in these latter cases, where sensitivity is usually limited by low metabolite concentrations and completing acquisitions within a single scan is not a primary concern, the single-instant nature of the spatially encoded compensation principle can be combined with the classical scheme of 2D NMR, to deliver a robust approach for correcting the inhomogeneities. In such cases one can envision a family of experiments where inhomogeneities acting over the course of the indirect domain, are corrected in advance and at the time of the excitation by a suitable polychromatic pulse [23] acting in a spatially-selective manner owing to the application of a strong magnetic field gradient (Fig. 5A). This in turn requires setting, for each $t_1$ increment within an otherwise freely evolving 2D acquisition, the phases of the individual $N$ components making the polychromatic excitation pulse according to

$$[\phi_{\mathrm{RF}}]_i = -O(r_i)\tau_p - t_1\Omega_{\mathrm{inh}}(r_i), \quad i = 1,\ldots,N, \tag{16}$$

where $\tau_p$ is the duration of the polychromatic pulse and $\{O(r_i) = \gamma G_e r_i + \Omega_{\mathrm{inh}}(r_i)\}_{i=1\ldots N}$ constitute the pulse's basic $N$ frequency elements. The position-dependent evolution phases introduced by the excitation gradient and the $\Omega_{\mathrm{inh}}(r)$ distribution would then cancel out at the culmination of the indirect-domain evolution period, enabling a high resolution signal $S(t_1)$ to be sampled. Repeating the procedure a suitable number of $t_1$ free evolution increments, should then yield a conventional high resolution time-domain signal when viewed along the indirect domain. Notice that since such signals can be observed while in the absence of ancillary field gradients no extra sensitivity penalties will be involved, and that since in general $\tau_p \ll t_1^{\max}$ no significant scaling of the shifts and $J$-couplings

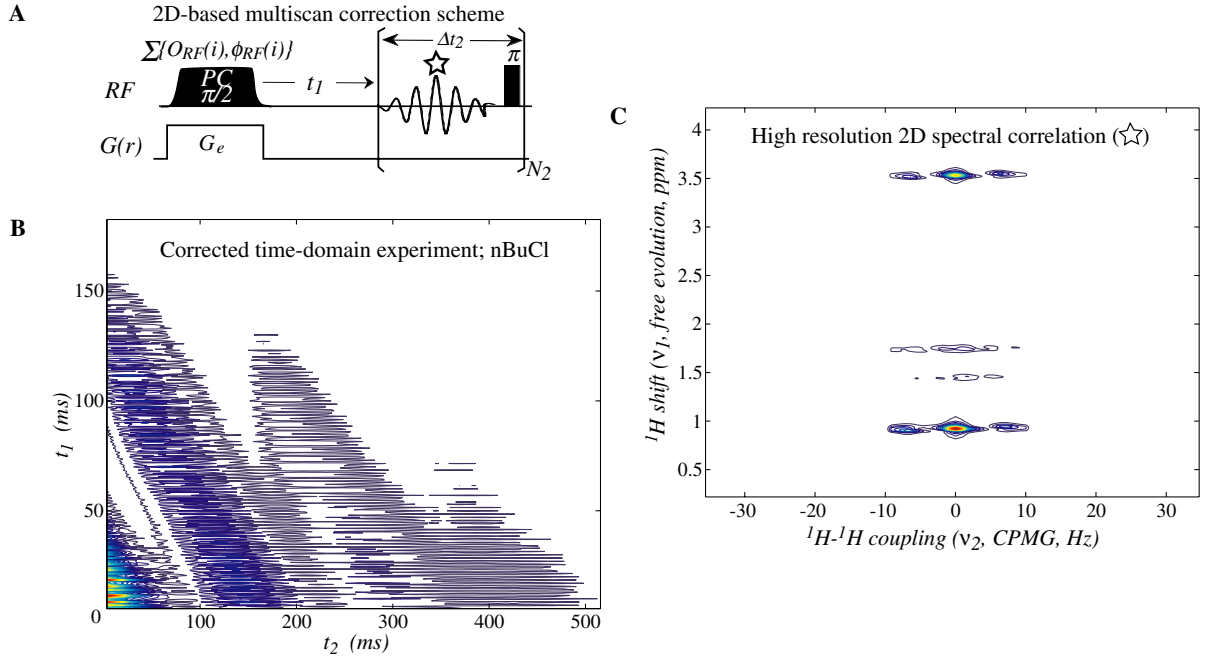


Fig. 5. (A) Novel scheme proposed for the refocusing of field inhomogeneities in a two-dimensional fashion, incorporating a spatially-encoded correction based on a polychromatic excitation triggering the $t_1$, followed by a CPMG-type signal acquisition (☆) for sensitivity enhancement happening over $t_2$. (B) Experimental time-domain results obtained with the pulse sequence shown in (A) on the artificially broadened sample shown in Fig. 3A; compare the time decays arising along these two axes with the one displayed for the same sample upon applying a conventional excitation (Fig. 6A). For all the 360 increments making up the resulting 2D data set, a polychromatic irradiation was built from 173 individual frequency components equally spaced over a ≈475 kHz spread, achieved by the application of a 60 G/cm gradient along the sample tube's $\hat{z}$ direction. The phases of the individual frequency components making up such compensating pulse were tailored according to the recipe in Eq. (16), with the $t_1$ parameter incremented in 500 μs steps. Although the pulses resulting by the addition of these components demanded an RF power that was unavailable for synthesizing π/2 nutations over the first few $t_1$ increments (≈100 W), this resulted in no significant distortions. Notice that the homonuclear $J$ modulation, with a period of ca 140 ms, is clearly discernible along both time domains. (C) 2D chemical/shift—$J$-coupling correlation spectrum arising from a suitable two-dimensional processing of the data set shown in (B). For the sake of simplicity this spectrum was retrieved from solely a single set of the points digitized during $t_2$, corresponding schematically to the positions indicated by the star. Sensitivity could be improved by processing all points within each $\Delta t_2$ period in a similar fashion, and then co-adding the resulting 2D spectra. As its time-domain counterpart (B), this 2D frequency spectrum is shown in magnitude mode.

from their free-evolution values will result. Thus are the main two drawbacks associated to the single-scan procedures described in the preceding Section, taken care of. Moreover, since in a general case inhomogeneities will lead to an effective decay time $T_2^* \ll T_2$, it becomes possible to monitor signals along the direct $t_2$ domain under the presence of a CPMG-type echo train—further enhancing the per-scan sensitivity [24,25]. All in all, if numerous individual scans are to be collected anyhow for the sake of signal averaging and if inhomogeneity is a substantial problem, it appears convenient to transform these scans into individual $t_1$ increments incorporating the inhomogeneity compensation scheme embodied by Eq. (16), rather than simply take their average as in a conventional 1D hard-pulse experiment.

To explore the compensation abilities of the scheme just described, a series of tests were carried out. An illustration of the experiment's performance is demonstrated in Figs. 5B and C, which summarize the 2D results arising from the $n$-butylchloride/$CDCl_3$ standard subject once again to a ca. 1.5 kHz inhomogeneity along the $\hat{z}$-axis. Although these inhomogeneities result in a conventional FID whose $T_2^*$ is only a few milliseconds long (Fig. 6A), signals evolving for hundreds of milliseconds along both $t_1$ and $t_2$ are obtained upon using the inhomogeneity compensation procedure (Fig. 6B). For this particular example the inhomogeneity averaging reflects the compensation introduced by a single, 400 μs long π/2 polychromatic pulse triggering the $t_1$ evolution, and the refocusing effects brought about by a train of hard CPMG π pulses executed every 4 ms during $t_2$. Notice that by virtue of the free evolution experienced by the spins during $t_1$ chemical shifts and $J$-couplings result in a spectrum with a completely normal appearance—yet with linewidths that are ca. 400 times sharper than in their single-pulse counterpart.

It follows that a spatially-encoded 2D corrective approach can significantly improve the appearance of spectroscopic NMR data without incurring in any apparent penalties—at least for cases where numerous scans are to be collected in any case for the sake of improving sensitivity. A question that then naturally arises concerns the potential limitations of this 2D inhomogeneity compensation procedure. In principle one could assume that, given an encoding gradient that is large enough compared to the local inhomogeneity and sufficient RF power to efficiently excite the resulting gradient-induced bandwidth,

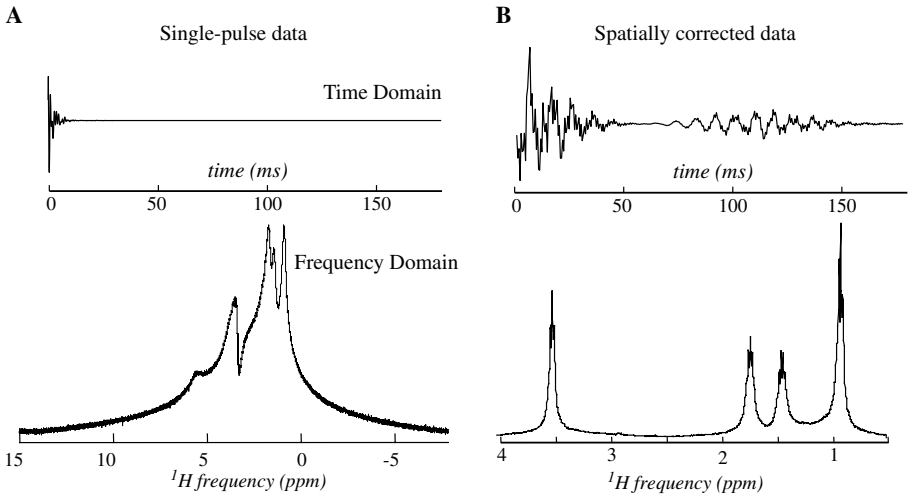


Fig. 6. Comparison between: (A) The single-pulse data $S(t)/I(\Omega_1)$ arising from the inhomogeneously-broadened *n*-butylchloride/$CDCl_3$ sample. (B) The $S(t_1)/I(\Omega_1)$ results achievable upon applying on the same sample the polychromatic 2D correction scheme. These latter traces correspond to a time-domain slice/frequency-domain projection of the 2D data shown in Fig. 5, along the indirect dimension.

arbitrarily large inhomogeneities could be compensated by the procedure. While at the same time, the low sensitivities following from the short $T_2^*$'s imposed by the magnet's inhomogeneities could be dealt with by the application of a signal-enhancing CPMG train. Given such considerations it appears that even currently-available commercial gradient probeheads, capable of reaching in excess of 2000 G/cm, could go to great lengths towards dealing with the ≈100 ppm inhomogeneities normally characterizing high-field Physics-oriented magnets. At some point, however, a new inhomogeneity-driven line broadening mechanism will arise, associated now to the *incoherent motions* that spins in a liquid will undergo over the course of the $t_1$ period—between the time they are excited, and the time when their coherent echo is detected. Such diffusion effects are known to inflict decays of the form $\exp[-D(\frac{\partial\Omega_{\text{inh}}}{\partial z})^2 t_1^3]$ onto a spins' evolution [26], and will eventually limit the accuracy with which field inhomogeneities can be refocused by the hereby proposed coherent manipulations. In order to get a better idea of the destructive effects imposed by such phenomena a series of numerical simulations were carried out based on a quadratic inhomogeneity (linear terms being usually minor close to the magnet's sweet spot and anyhow addressable by linear compensating gradients). It was found that when having $G_e \approx 2000$ G/cm gradients available for doing the compensation, ≈50 kHz wide heterogeneities (100 ppm at 11.7 T over the full sample volume) could be reduced to ca. 30 Hz line widths in the resolved 2D peaks—this residual reflecting the action of diffusive effects placing an ultimate limit on the spatial refocusing.

## 4. Conclusions

By treating the sample in a spatially-selective fashion, the combined application of external field gradients and of frequency-selective pulses opens up a number of new opportunities towards the acquisition of high resolution NMR spectra within inhomogeneous fields. To demonstrate this the present study employed artificially-broadened 1D models where inhomogeneities had been a priori mapped, a knowledge which is relatively straightforward to obtain whenever the available gradients exceed the internal field distortions. A series of single- and multiple-scan compensating alternatives could then be proposed. The former have obvious speed advantages, but achieve their aim at the expense of either sensitivity or resolution limitations. For low-sensitivity, low-field cases where signal averaging may anyhow be required and where chemical shift resolution is at a premium, such sacrifices may be unacceptable. An alternative was thus presented based on merging multiscan acquisitions with the spatially-encoded inhomogeneity-compensation procedure, within the framework of a traditional 2D NMR experiment. The resulting compensation is then endowed with a good sensitivity by virtue of the summations involved in the $t_1$ Fourier transformation and the $t_2$ CPMG acquisition, together with an unscaled spectral information reflecting the free evolution occurring along $t_1$. A further homonuclear *J*-domain encoding, unimportant at high $B_o$ fields but potentially diagnostic at lower fields [27], also arises along the direct domain. All these features combined could proof particularly useful in a number of scenarios including in vivo analyses of metabolites in animal or human scanners; studies that are generally characterized by relatively high heterogeneities, limited shimming capabilities, and relatively low magnetic fields where chemical shift displacements are at a premium.

A number of simplifications adopted throughout the present study are worth remarking. One involved the $B_o$ inhomogeneities, which were assumed one-dimensional and time independent. Another concerned the RF manipulations, which were assumed to act instantaneously and on the basis of the small-angle approximation. While these assumptions were taken for the sake of evidencing more

clearly the nature of the compensation procedures, none of them is actually essential and all can be dispensed of in realistic applications. From a practical standpoint, the greatest challenge is probably posed by the extension of the procedure hereby described from one spatial dimension to three. There are a number of different ways by which such extension can be carried out; these range from transforming the single-axis compensation procedure into a multiple-axis one where multiple corrective RF pulses are applied while under the action of linearly-independent gradients, to the design of a compensation procedure based on the application of a single multi-dimensional corrective RF pulse. The first of these approaches could be readily incorporated into standard spectroscopic sequences such as STEAM or PRESS [3], yet the nature of $\Omega_{\text{inh}}(r)$ profiles that could be thus compensated is mostly limited to products of 1D field inhomogeneities. The latter approach by contrast would be truly general, yet given the lengthier nature of multidimensional RF pulses vis-à-vis their 1D counterparts [28] it could be more susceptible to signal losses. In-between solutions, involving sequential 1D and 2D RF compensating pulses, could constitute a good compromise to overcome these limitations. The single-instant nature of the various schemes hereby discussed also makes them suitable for dealing with periodic time-dependent $B_o$ variations, provided these are amenable to characterizations by means navigator scans [29]. As for the design of all our RF compensations based on the small angle approximation, it is also worth noting that numerous different alternatives discussed in the literature are worth exploring within an inhomogeneity compensation context [28]. Examples on the implementation and potential of these various kinds of improvements will be reported in an upcoming study.

## Acknowledgments

We are grateful to Mr. Assaf Tal (WIS) for valuable comments during the course of this study. This work was supported by the Israel Science Foundation (ISF 1206/05), the German-Israel Fund (GIF 782/2003) and the US National Institutes of Health (GM-72565).

## References

[1] D.M. Grant, R.K. Harris (Eds.), Encyclopedia of NMR, John Wiley, Chichester, 1996.
[2] D.D. Laukien, W.H. Tschopp, Superconducting NMR magnet design, Concepts Magn. Reson. 6 (1994) 255–273.
[3] D.D. Stark, W.G. Bradley (Eds.), Magnetic Resonance Imaging, third ed., Mosby, St. Louis, 1999, pp. 181–214.
[4] P.J. McDonald, Stray field magnetic resonance imaging, Prog. Nucl. Magn. Reson. Spectrosc. 30 (1997) 69–99.
[5] D.P. Weitekamp, J.R. Garbow, J.B. Murdoch, A. Pines, High resolution NMR spectra in inhomogeneous magnetic fields: applications of total spin coherence transfer echoes, J. Am. Chem. Soc. 103 (1981) 3578–3580.
[6] J.J. Balbach, M.S. Conradi, D.P. Cistola, C.G. Tang, J.R. Garbow, W.C. Hutton, High resolution NMR in inhomogeneous fields, Chem. Phys. Lett. 277 (1997) 367–374.
[7] S. Vathyam, S. Lee, W.S. Warren, Homogeneous NMR spectra in inhomogeneous fields, Science 272 (1996) 92–96.
[8] Y. Lin, S. Ahn, N. Murali, W. Brey, C.R. Bowers, W.S. Warren, High resolution >1 GHz NMR in unstable magnetic fields, Phys. Rev. Lett. 85 (2000) 3732–3735.
[9] C.A. Meriles, D. Sakellariou, H. Heise, A.J. Moulé, A. Pines, Approach to high resolution ex situ NMR spectroscopy, Science 293 (2001) 82–85.
[10] J. Perlo, V. Demas, F. Casanova, C.A. Meriles, J. Reimer, A. Pines, B. Blümich, High resolution NMR spectroscopy with a portable single-sided sensor, Science 308 (2005) 1278–1279.
[11] B. Shapira, L. Frydman, Spatial encoding and the acquisition of high resolution NMR spectra in inhomogeneous magnetic fields, J. Am. Chem. Soc. 126 (2004) 7184–7185.
[12] D. Topgaard, R.W. Martin, D. Sakellariou, C.A. Meriles, A. Pines, "Shim pulses" for NMR spectroscopy and imaging, Proc. Natl. Acad. Sci. USA 101 (2004) 17576–17581.
[13] N. Chen, A. Wyrwicz, Removal of intravoxel dephasing artifact in gradient-echo images using a field-map based RF refocusing technique, Magn. Reson. Med. 42 (1999) 807–812.
[14] V.A. Stenger, F.E. Boada, D.C. Noll, 3D tailored RF pulses for the reduction of susceptibility artifacts in $T_2^*$-weighted functional MRI, Magn. Reson. Med. 44 (2000) 525–531.
[15] L. Frydman, T. Scherf, A. Lupulescu, The acquisition of multidimensional NMR spectra within a single scan, Proc. Natl. Acad. Sci. USA 99 (2002) 15858–15862.
[16] L. Frydman, T. Scherf, A. Lupulescu, Principles and features of single-scan two-dimensional NMR spectroscopy, J. Am. Chem. Soc. 125 (2003) 9204–9217.
[17] Y. Shrot, B. Shapira, L. Frydman, Ultrafast 2D NMR spectroscopy using a continuous spatial encoding of the spin interactions, J. Magn. Reson. 171 (2004) 162–169.
[18] P. Pelupessy, Adiabatic single-scan 2D NMR spectroscopy, J. Am. Chem. Soc. 125 (2003) 12345–12350.
[19] A. Tal, B. Shapira, L. Frydman, A continuous phase-modulated approach to spatial encoding in ultrafast 2D NMR spectroscopy, J. Magn. Reson. 176 (2005) 107–114.
[20] N.S. Andersen, W. Kockenberger, A simple approach for phase-modulated single-scan 2D NMR spectroscopy, Magn. Reson. Chem. 43 (2005) 795–797.
[21] A. Tal, L. Frydman, Spatial encoding and the single-scan acquisition of high definition MR images in inhomogeneous magnetic fields, J. Magn. Reson., in press.
[22] B. Shapira, A. Lupulescu, Y. Shrot, L. Frydman, Line Shape Considerations in Ultrafast 2D NMR, J. Magn. Reson. 166 (2004) 152–163.
[23] E. Kupce, R. Freeman, Pulse design in the frequency domain, J. Magn. Reson. A 103 (1993) 358–363.
[24] S. Meiboom, D. Gill, Modified spin-echo method for measuring nuclear relaxation times, Rev. Sci. Instrum. 29 (1959) 688–691.
[25] R. Siegel, T.T. Nakashima, R. Wasylishen, Signals-to-noise enhancement of NMR spectra of solids using multiple-pulse spin-echo experiments, Concepts Magn. Reson. 26A (2005) 62–77.
[26] H.Y. Carr, E.M. Purcell, Effects of diffusion on free precession in nuclear magnetic resonance experiments, Phys. Rev. 94 (1954) 630–638.
[27] R.E. Hurd, J. Kurhanewicz, Single voxel oversampled J-resolved spectroscopy of in vivo human prostate tissue, Magn. Reson. Med. 45 (2001) 973–980.
[28] M.A. Bernstein, K.F. King, X.J. Zhou, Handbook of MRI Pulse Sequences, Academic, New York, 2004.
[29] T.S. Sachs, C.H. Meyer, J. Kohlu, D.G. Nishimura, A. Macovski, Real-time motion detection in spiral MRI using navigators, Magn. Reson. Med. 32 (1994) 639–645.